

The mesoscale eddies and Kuroshio transport in the western North Pacific east of Taiwan from 8-year (2003–2010) model reanalysis

I-Huan Lee · Dong Shan Ko · Yu-Huai Wang ·
Luca Centurioni · Dong-Ping Wang

Received: 14 June 2012 / Accepted: 30 June 2013 / Published online: 25 July 2013
© The Author(s) 2013. This article is published with open access at Springerlink.com

Abstract The relationship between the Kuroshio volume transport east of Taiwan ($\sim 24^\circ\text{N}$) and the impinging mesoscale eddies is investigated using 8-year reanalysis of a primitive equation ocean model that assimilates satellite altimetry and SST data. The mean and fluctuations of the model Kuroshio transport agree well with the available observations. Analysis of model dynamic heights and velocity fields reveals three dominant eddy modes. The first mode describes a large eddy of ~ 500 km in diameter, centered at $\sim 22^\circ\text{N}$. The second mode describes a pair of the north–south counter-rotating eddies of ~ 400 km in diameter each, centered at 23° and 20°N , respectively. The third mode describes a pair of the east–west counter-rotating eddies of ~ 300 km in diameter each, centered at 21°N . The associated velocity fields

indicate eddies extending to 600–700 m in depth with vertical shears concentrated in the upper 400 m. All three modes and the model Kuroshio transport have similar dominant time-scales of 70–150 days and generally are coherent. The decreased Kuroshio volume transports typically are associated with the impinging cyclonic eddies and the increased transports with the anticyclonic eddies. Selected drifter trajectories are presented to illustrate the three eddy modes and their correspondence with the varying Kuroshio transports.

Keywords Western North Pacific · Mesoscale eddy · Kuroshio transport · EOF · SVD

Responsible Editor: Anthony C. Hirst

I-H. Lee
Department of Marine Environment and Engineering, National Sun
Yet-sen University, Kaohsiung, Taiwan, Republic of China
e-mail: ihlee@mail.nsysu.edu.tw

D. S. Ko
Naval Research Laboratory, John C. Stennis Space Center,
MS, USA
e-mail: ko@mrlssc.navy.mil

Y.-H. Wang (✉)
Institute of Applied Marine Physics and Undersea Technology/
Department of Oceanography, National Sun Yet-sen University,
Kaohsiung, Taiwan,
Republic of China
e-mail: yhwang@faculty.nsysu.edu.tw

L. Centurioni
Scripps Institution of Oceanography, UCSD, La Jolla, CA, USA
e-mail: lcenturioni@ucsd.edu

D.-P. Wang
School of Marine and Atmospheric Sciences,
Stony Brook, NY, USA
e-mail: dong-ping.wang@stonybrook.edu

1 Introduction

Mesoscale eddies are abundant in the ocean. Chelton et al. (2007), based on 10 years of altimetry sea surface height anomaly (SSHA) data, indicated that more than 50 % of low-frequency variability over much of the ocean can be accounted for by eddies with diameters of 100–200 km and amplitudes of 5–25 cm. These eddies propagate nearly due west at approximately the phase speed of nondispersive baroclinic Rossby waves (Barron et al. 2009). In the western North Pacific, the most energetic eddy activity is in the Kuroshio Extension. There is yet another zonal band in the subtropical gyre between 19° and 25°N where energetic eddy activities are attributed to the baroclinic instabilities in the Subtropical Countercurrent (e.g., Qiu 1999; Kobashi and Kawamura 2002; Qiu and Chen 2010; Rudnick et al. 2011). The dominant eddy time scale in the STCC is ~ 100 days and their westward propagating speed is ~ 8 km/day (Qiu and Chen 2010). Most of the eddies are concentrated near 22°N , and many may reach the Kuroshio off the eastern coast of Taiwan (Hwang et al. 2004). Roemmich and Gilson (2001) presented hydrographic evidence for mesoscale eddies in the STCC based on repeat

Report Documentation Page				Form Approved OMB No. 0704-0188	
Public reporting burden for the collection of information is estimated to average 1 hour per response, including the time for reviewing instructions, searching existing data sources, gathering and maintaining the data needed, and completing and reviewing the collection of information. Send comments regarding this burden estimate or any other aspect of this collection of information, including suggestions for reducing this burden, to Washington Headquarters Services, Directorate for Information Operations and Reports, 1215 Jefferson Davis Highway, Suite 1204, Arlington VA 22202-4302. Respondents should be aware that notwithstanding any other provision of law, no person shall be subject to a penalty for failing to comply with a collection of information if it does not display a currently valid OMB control number.					
1. REPORT DATE 25 JUL 2013		2. REPORT TYPE		3. DATES COVERED 00-00-2013 to 00-00-2013	
4. TITLE AND SUBTITLE The mesoscale eddies and Kuroshio transport in the western North Pacific east of Taiwan from 8-year (2003-2010) model reanalysis				5a. CONTRACT NUMBER	
				5b. GRANT NUMBER	
				5c. PROGRAM ELEMENT NUMBER	
6. AUTHOR(S)				5d. PROJECT NUMBER	
				5e. TASK NUMBER	
				5f. WORK UNIT NUMBER	
7. PERFORMING ORGANIZATION NAME(S) AND ADDRESS(ES) Naval Research Laboratory,1005 Balch Boulevard,Stennis Space Center,MS,39529				8. PERFORMING ORGANIZATION REPORT NUMBER	
9. SPONSORING/MONITORING AGENCY NAME(S) AND ADDRESS(ES)				10. SPONSOR/MONITOR'S ACRONYM(S)	
				11. SPONSOR/MONITOR'S REPORT NUMBER(S)	
12. DISTRIBUTION/AVAILABILITY STATEMENT Approved for public release; distribution unlimited					
13. SUPPLEMENTARY NOTES					
14. ABSTRACT The relationship between the Kuroshio volume transport east of Taiwan (~24°N) and the impinging mesoscale eddies is investigated using 8-year reanalysis of a primitive equation ocean model that assimilates satellite altimetry and SST data. The mean and fluctuations of the model Kuroshio transport agree well with the available observations. Analysis of model dynamic heights and velocity fields reveals three dominant eddy modes. The first mode describes a large eddy of ~500 km in diameter, centered at ~22° N. The second mode describes a pair of the north-south counter-rotating eddies of~400 km in diameter each, centered at 23° and 20° N, respectively. The third mode describes a pair of the east-west counter-rotating eddies of~300 km in diameter each, centered at 21° N. The associated velocity fields indicate eddies extending to 600-700 m in depth with vertical shears concentrated in the upper 400 m. All three modes and the model Kuroshio transport have similar dominant timescales of 70-150 days and generally are coherent. The decreased Kuroshio volume transports typically are associated with the impinging cyclonic eddies and the increased transports with the anticyclonic eddies. Selected drifter trajectories are presented to illustrate the three eddy modes and their correspondence with the varying Kuroshio transports.					
15. SUBJECT TERMS					
16. SECURITY CLASSIFICATION OF:			17. LIMITATION OF ABSTRACT Same as Report (SAR)	18. NUMBER OF PAGES 14	19a. NAME OF RESPONSIBLE PERSON
a. REPORT unclassified	b. ABSTRACT unclassified	c. THIS PAGE unclassified			

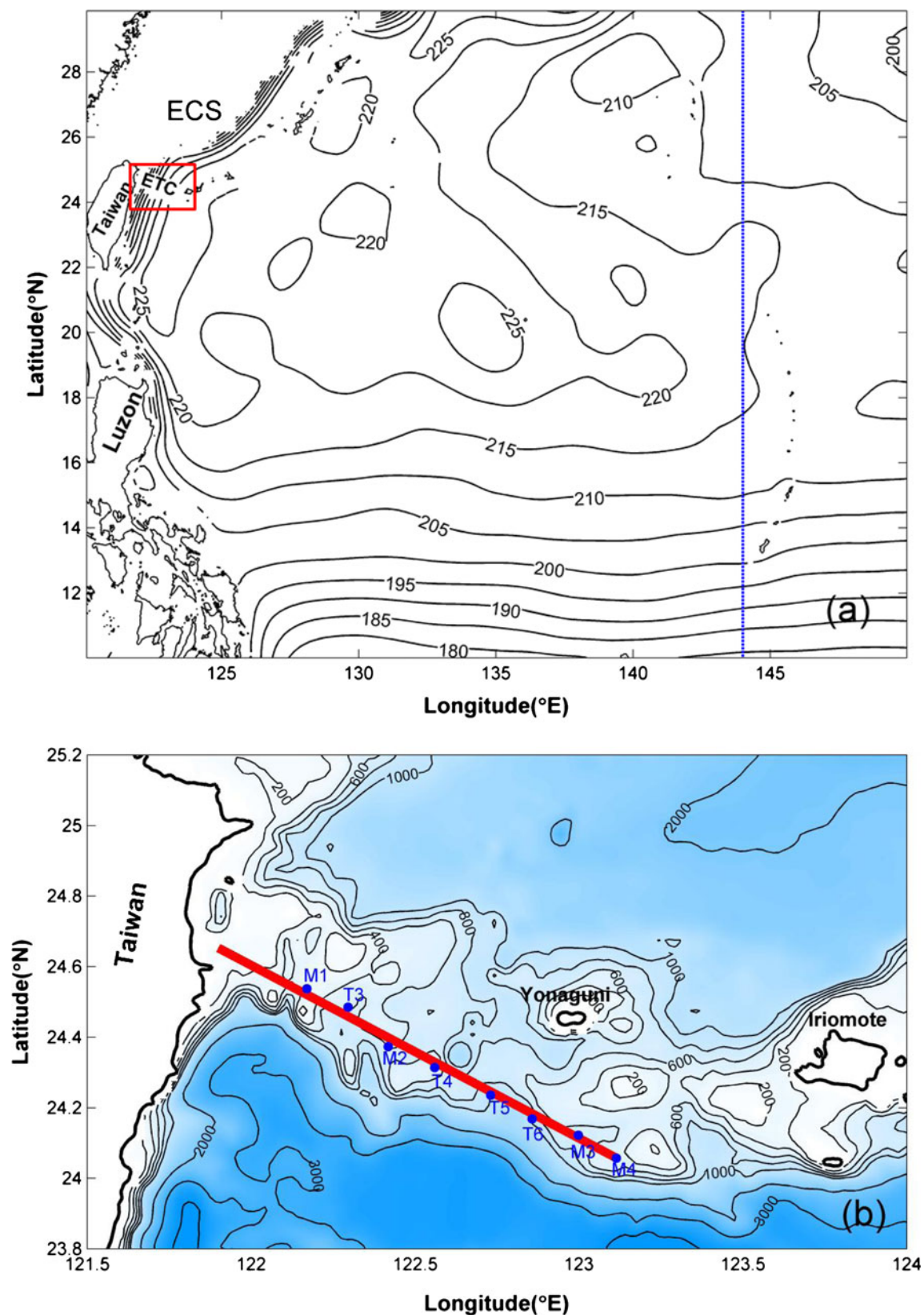


Fig. 1 **a** Mean model dynamic heights referenced to 1,000 dbar. The red box marks the ETC shown in **b**. **b** Topographic map of the ETC (depth contour interval within 1,000 m is 200 m). The transport integrated section is marked by the red line. Mooring stations M1–M4 of

PCM-1 are marked by the blue dots. **c** Longitudinal cross-section (144°E, dotted blue line in **a**) of temperature (blue contours in °C) and zonal velocity (black contours in m/s, positive is eastward)

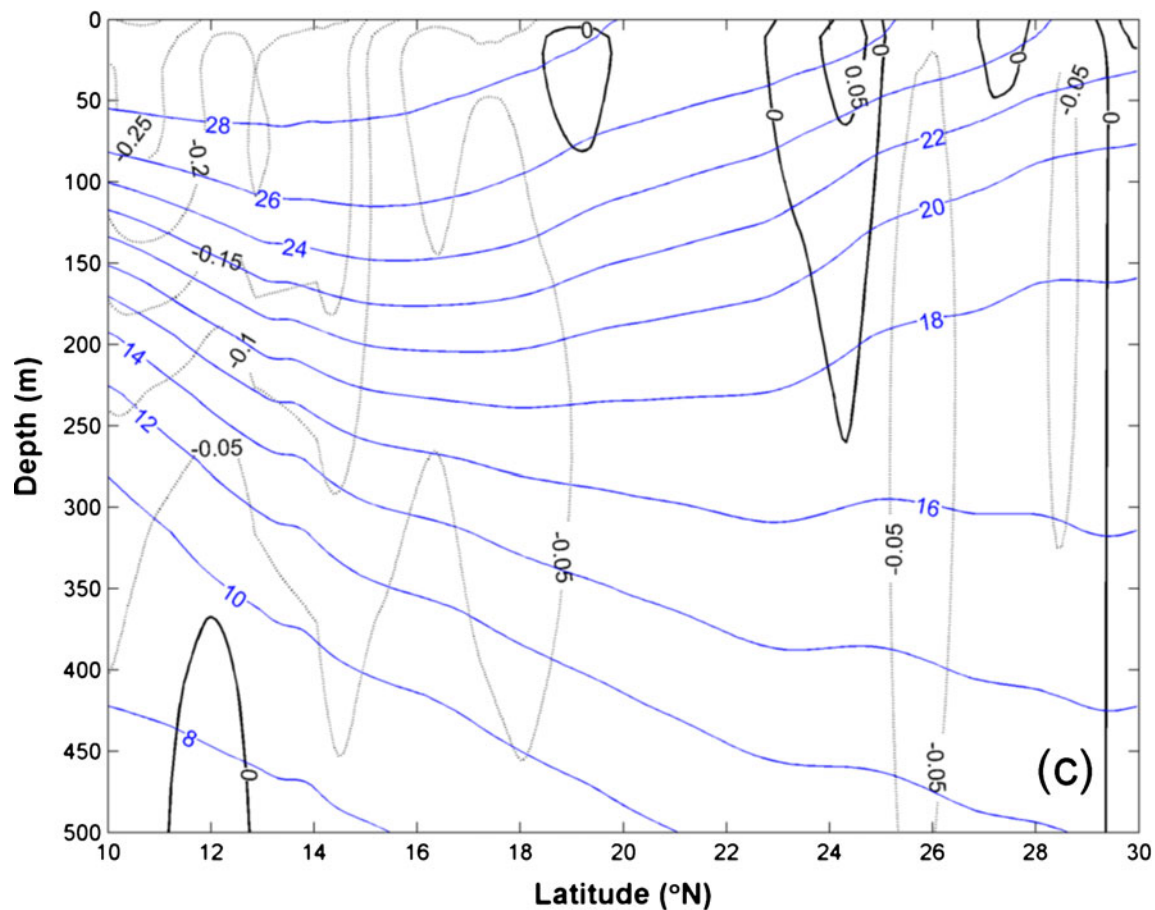


Fig. 1 (continued)

high-resolution expendable bathythermograph (XBT) transects between Guam and Hong Kong. They found an eddy-rich latitude at $\sim 20^\circ$ N. The typical eddy size is about 500 km with a peak-to-trough temperature difference of 2.2°C in the center of the thermocline. Lee et al. (2003) investigated the time history and vertical structure of a large cyclonic eddy using XBT and Topex/Poseidon altimetry data. They suggested that cyclonic eddies could be also generated by slowly moving typhoons.

The impact of eddies on the Kuroshio volume transport has long been recognized (Yang et al. 1999; Zhang et al. 2001). The Kuroshio originates east of the Philippines, flows along the east coasts of Luzon and Taiwan, and enters the East China Sea (ECS) through the East Taiwan Channel (ETC), a narrow (< 150 km) ridge between the northeastern coast of Taiwan and the southern tip of the Ryukyu Islands (Fig. 1). During the World Ocean Circulation Experiment, the Kuroshio volume transport was monitored in the ETC with a dense array of current meter moorings, the PCM-1 (Fig. 1b), for about 20 months from September 1994 to May 1996 (Johns et al. 2001; Zhang et al. 2001). The observed volume transport had a mean of 21.5 Sv ($1\text{ Sv}=10^6\text{ m}^3/\text{s}$) and significant 100-day timescale fluctuations with amplitudes as large as 10 Sv. For comparison, the Florida

Current has a larger mean transport (31.7 Sv) but much smaller eddy timescale fluctuations (Leaman et al. 1995; Lee et al. 2001). The difference between these two western boundary current systems suggests that the Kuroshio system is strongly impacted by the westward propagating mesoscale eddies (Yang et al. 1999; Zhang et al. 2001; Gawarkiewicz et al. 2011).

Qiu and Chen (2010) described the “eddy rich” and “eddy weak” years in the STCC ($19\text{--}25^\circ$ N, $135\text{--}175^\circ$ E). Chang and Oey (2011) found that the interannual Kuroshio transports estimated from sea level differences between Keelung and Ishigaki are highly correlated with the STCC variability. The Kuroshio transport lags the STCC variation by 6–8 months at $\sim 132^\circ$ E, and the time lag increases eastward. Chang and Oey (2012) introduced the Philippines–Taiwan Oscillation (PTO), a climate index that relates the interannual variation of the STCC eddy activities and Kuroshio transports to the large-scale wind stress curl over the subtropical western North Pacific (also see Qiu and Chen 2010). The Kuroshio Current also experiences strong interannual variability further downstream in the ECS (Liu and Gan 2012). Ichikawa et al. (2008) and Hsin et al. (2011) showed that the Kuroshio variations in ECS were induced by mesoscale eddies east of Taiwan.

The relationship between the Kuroshio transport and mesoscale eddies east of Taiwan was examined from PCM-1 observations. Yang et al. (1999) suggested that impinging anticyclonic eddies resulted in an increase of the Kuroshio transport. Zhang et al. (2001), on the other hand, found that anticyclonic eddies caused a decrease in the Kuroshio transport. Also, Gawarkiewicz et al. (2011) found a maximum correlation of 0.83 between PCM-1 Kuroshio transport and SSHa at 23.9° N, 123.2° E. There were other studies that utilized direct velocity/transport measurements. Andres et al. (2008a) illustrated three events of the approaching anticyclonic (cyclonic) eddies that increased (decreased) the transports in the ECS through the Kerama Gap. Also, Zhu et al. (2004) showed that the approaching anticyclonic/cyclonic eddies increased/decreased the volume transport southeast of Okinawa Island.

Maps of sea level anomaly such as those produced by Archiving, Validation and Interpretation of Satellite Oceanographic data (AVISO) are often used in studies of the large-scale flow variability (e.g. Centurioni et al. 2008; Maximenko et al. 2009). The altimetry spatial resolution, however, is too coarse to map the Kuroshio transport. During the Jason 1-Topex/Poseidon tandem mission, the spatial resolution is improved, but the record is too short (Scharffenberg and Stammer 2010). The direct Kuroshio volume transport measurement is difficult, and the record length is too short compared to the typical eddy timescales (Johns et al. 2001). In this study, we analyze the Kuroshio transport variability using 8 years (2003–2010) of reanalysis product from a high-resolution regional ocean model, the East Asian Seas Nowcast/Forecast System (EASNFS) of the US Naval Research Laboratory (NRL) (Rhodes et al. 2002; Ko et al. 2009) (http://www7320.nrlssc.navy.mil/NLIWI_WWW/EASNFS_WWW/EASNFS_intro.html). Unlike the previous ~20-month

PCM-1 transport measurements, the 8-year EASNFS reanalysis time period is considerably longer than the eddy timescales. Our goal is to identify patterns of eddy variability east of Taiwan to better describe their relationship with the Kuroshio transport variability. We demonstrate that the mean and fluctuations of the Kuroshio transport from the reanalysis are fully consistent with the statistics derived from the PCM-1. We show that the eddy kinetic energy (EKE) from the reanalysis agrees with that calculated from the altimetry. Moreover, we validate the model eddy flow fields with selected drifter trajectories from the Global Drifter Program (GDP). Unlike previous studies based on either sea level anomalies or short-volume transport measurements, our study provides a much more coherent description of the Kuroshio transport and the impinging mesoscale eddies east of Taiwan. In particular, we are able to resolve the long-standing controversy from the PCM-1 study about the role of the anticyclonic/cyclonic eddies on the Kuroshio transport variations.

2 Methods

The EASNFS is an application of NRL Ocean Nowcast/Forecast System (Ko et al. 2008). The ocean model in the EASNFS is the Navy Coastal Model (Martin 2000) which is adopted from the Princeton Ocean Model (POM) with modifications to accommodate data assimilation, hybrid vertical coordinates, and multiple nesting. A statistical regression model, the Modular Ocean Data Assimilation System (Carnes et al. 1996; Fox et al. 2002), based on historical observations, is used to produce the three-dimensional ocean temperature and salinity analyses from satellite altimetry and Multi-Channel Sea Surface Temperature (MCSST). EASNFS

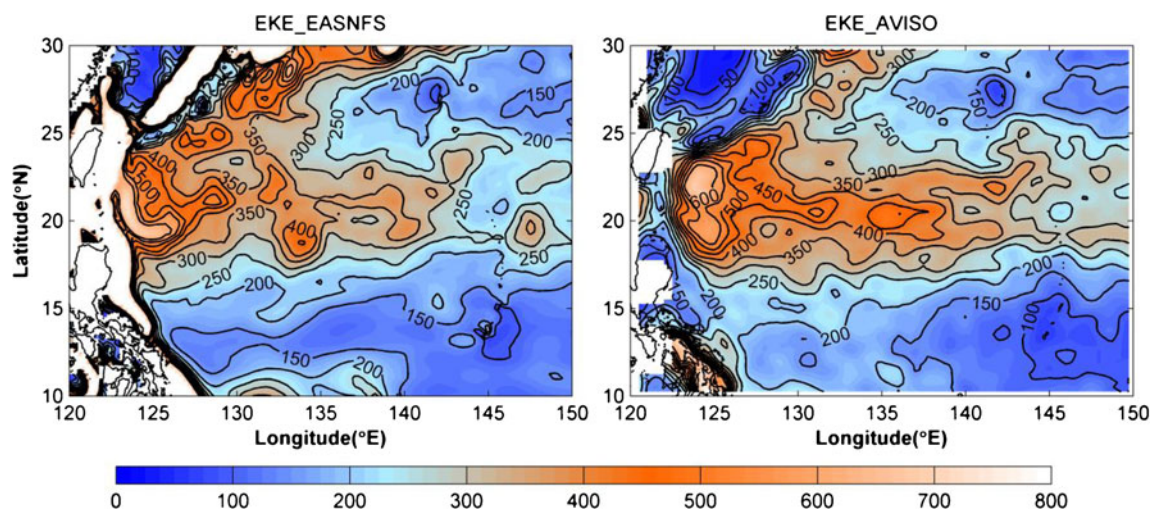


Fig. 2 Mean EKE derived from model results (*left*) and AVISO altimetry (*right*). Contour lines range from 0 to 600 with an interval of 50. The unit is cm^2/s^2 . Values greater than 800 are assigned to the same color of 800

assimilates the analyses by continuous modification of model temperature and salinity toward the analyses using a vertical weighting function that reflects the oceanic temporal and spatial correlation scales and the relative confidence between the model forecasts and analyses (Chapman et al. 2004; Ko et al. 2008).

Surface forcing of wind stress, heat flux, solar radiation, and surface atmospheric pressure, is derived from the Navy Operational Global Atmospheric Prediction System (Rosmond 1992). In the heat flux, solar radiation is retained separately, while the rest is adjusted by the differences between model sea surface temperature (SST) and MCSST and between model SST and seasonal climatology. The surface salt flux is estimated from the differences between model sea surface salinity (SSS) and the analysis and between model SSS and seasonal climatology (Ko et al. 2008). Jerlov (1964) type IA water is applied for solar extinction. Relaxation time of 5 and 30 days is used for adjustment of MCSST and seasonal SST climatology, respectively, and

relaxation time of 15 and 30 days is used for adjustment of SSS and seasonal SSS climatology, respectively.

The full EASNFS modal domain covers from 17.3° S to 52.2° N and from 99.2° E to 158.2° E. The horizontal resolution is ~1/12 degree that ranges from ~9.8 km at the equator to ~6.5 km at the model's northern boundary. The horizontal resolution is about 9 km in the study region. Temporal resolution is the 5-day averaged model field. There are 41 sigma- z levels with denser levels in the upper water column to better resolve the upper ocean. EASNFS analysis has been previously applied for several studies in the western North Pacific, e.g., the currents in the Korea/Tsushima Strait (Jacobs et al. 2005; Teague et al. 2006), transports in the Gulf of Papua (Keen et al. 2006), impact of typhoons on the upper ocean temperature (Lin et al. 2008), and thermal structures in South China Sea (Chang et al. 2010). We used the first 8 years (2003–2010) of the EASNFS reanalysis product in this study. The sea surface height (SSH) from the EASNFS analysis is

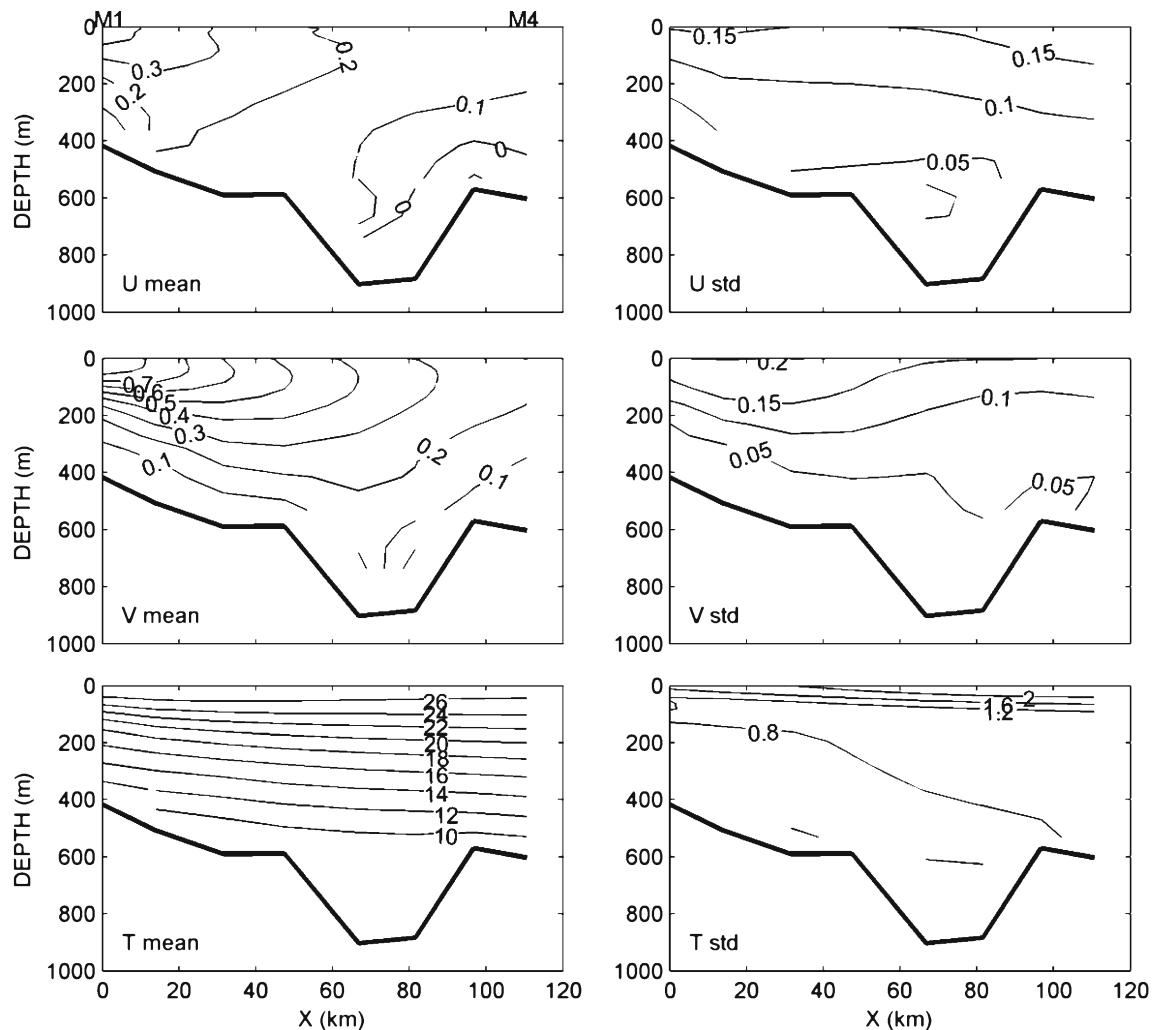


Fig. 3 Mean (left) and standard deviation (right) of velocities (U , V) and temperature (T) along PCM-1 from model results. PCM-1 stations M1 and M4 corresponding to each subplot are marked on the first subplot

highly correlated ($\gamma=0.84$) with the altimetry gridded data. In this study, the dynamic height calculated from the EASNFS temperature and salinity fields is used to describe the SSH in order to avoid effects due to large-scale barotropic fluctuations. The spatial and temporal patterns of dynamic heights are determined using the Empirical Orthogonal Functions (EOF) analysis. Also, the relationship between dynamic heights and model currents are analyzed with a covariance analysis that is effective in extracting the coherent structures of two diverse fields. The method was first introduced into climate research by Bretherton et al. (1992), and the term “singular value decomposition (SVD) analysis” was used. The oceanographic application can be found, for example, in Wang et al. (2003).

3 Results

Figure 1a shows model mean dynamic height (reference level=1,000 db) averaged over 8 years (2003–2010) in 10–30° N and 120–150° E. The Kuroshio and the North Equatorial Current (NEC) are clearly identified; the maximum

dynamic height is about 230 cm, located east of Ryukyu Islands. The NEC bifurcation near 14° N is also quite noticeable. The model mean dynamic height agrees well with the climatological estimates of Qiu (1999) and Rio et al. (2011), with significant details such as the strength of the STCC feature generally lying within the range of estimates. Figure 1c shows a cross-section of mean temperature and zonal velocity at 144° E. The STCC at 24° N is indicated by a weak eastward current in the upper 300 m and the corresponding uplifting isotherms. The model STCC temperature and velocity distributions also agree well with the observations presented in Qiu and Chen (2010). Figure 2 shows a comparison of the EKE from the model and altimetry. Both are averaged over 8 years (2003–2010), with a 120-h filter to remove the short-term fluctuations. The two have similar patterns except in the Kuroshio region where the altimetry is known to underestimate the EKE (e.g., Centurioni et al. 2008), mainly because of its inadequate spatial resolution. The spatial resolution of the merged data set is estimated to be ~150 km by Ducet et al. (2000), which is about the same as the width of Kuroshio at the region.

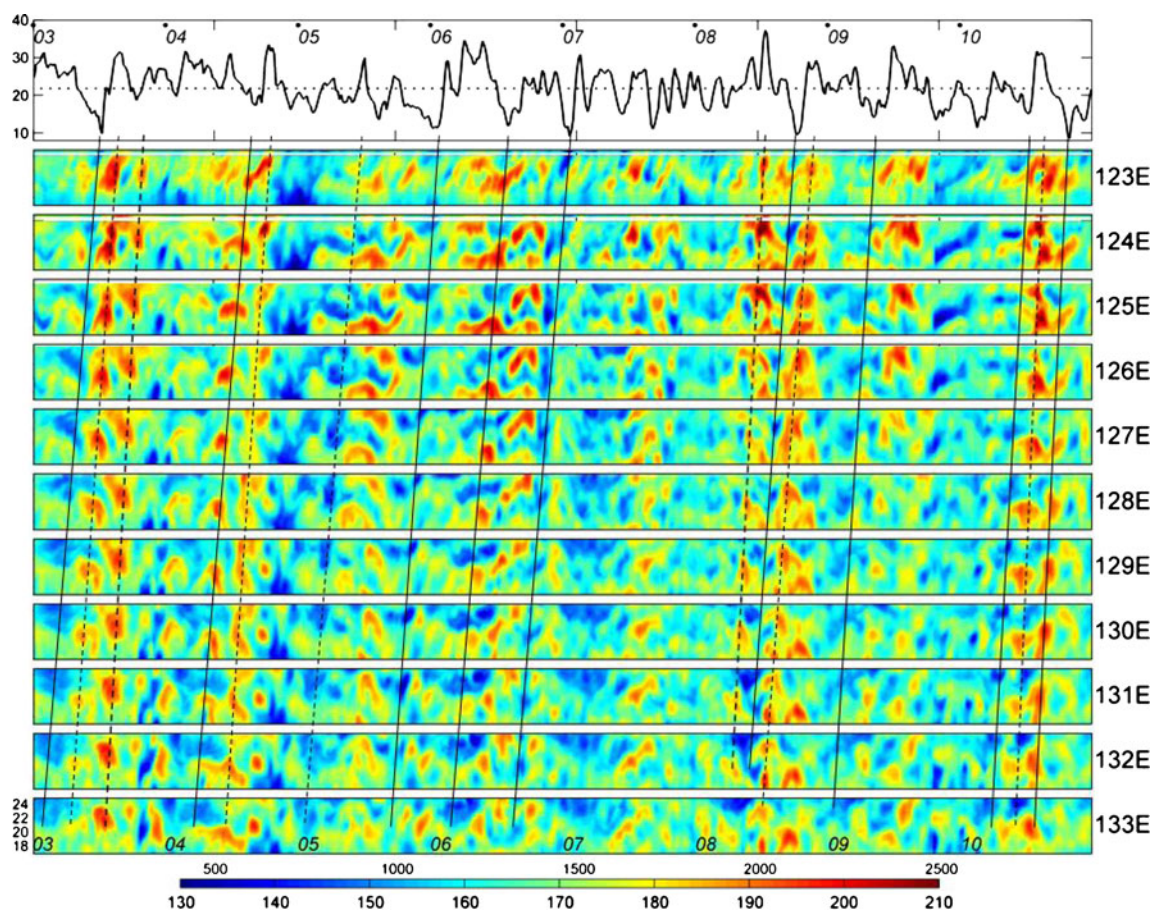


Fig. 4 The Kuroshio volume transport at PCM-1 from model results (*uppermost panel*, unit in Sv) and latitude–time plots of model dynamic heights for longitudes 133–123°E. Mean truncated PCM1 transport is marked by the *dotted line* at the *uppermost panel*. The *tilted solid/dashed*

lines mark the propagating eddies related to the Kuroshio lows/highs. Every January 1 from 2003 to 2010 in the time axis are marked with numbers 03~10 and also *dots* on the *top panel*

The model output is interpolated to the mooring locations (M1 to M4) of the PCM-1 array (Fig. 1b; Zhang et al. 2001). To compare with observation (Fig. 2 in Zhang et al. 2001), Fig. 3 shows across-stream structures of model mean and standard deviation for eastward (U) and northward (V) velocities and temperature (T). The mean V field shows the core (“main axis”) of the Kuroshio about 100 km in width and 400 m in depth, located in the western half of the channel. The mean U field is dominated by a weak eastward flow over

the entire section, with larger values (~ 0.3 m/s) in the western half of the channel. The base of the main thermocline (16°C) rises from about 300 m in depth at the eastern side to 200 m at the western side. The corresponding vertical shears are also stronger on the western side. Standard deviations of U and V are comparable along the entire section. The standard deviation of U increases eastward and intensifies near the surface, and the standard deviation of V has a core (~ 0.2 m/s) in the western half of the channel. The

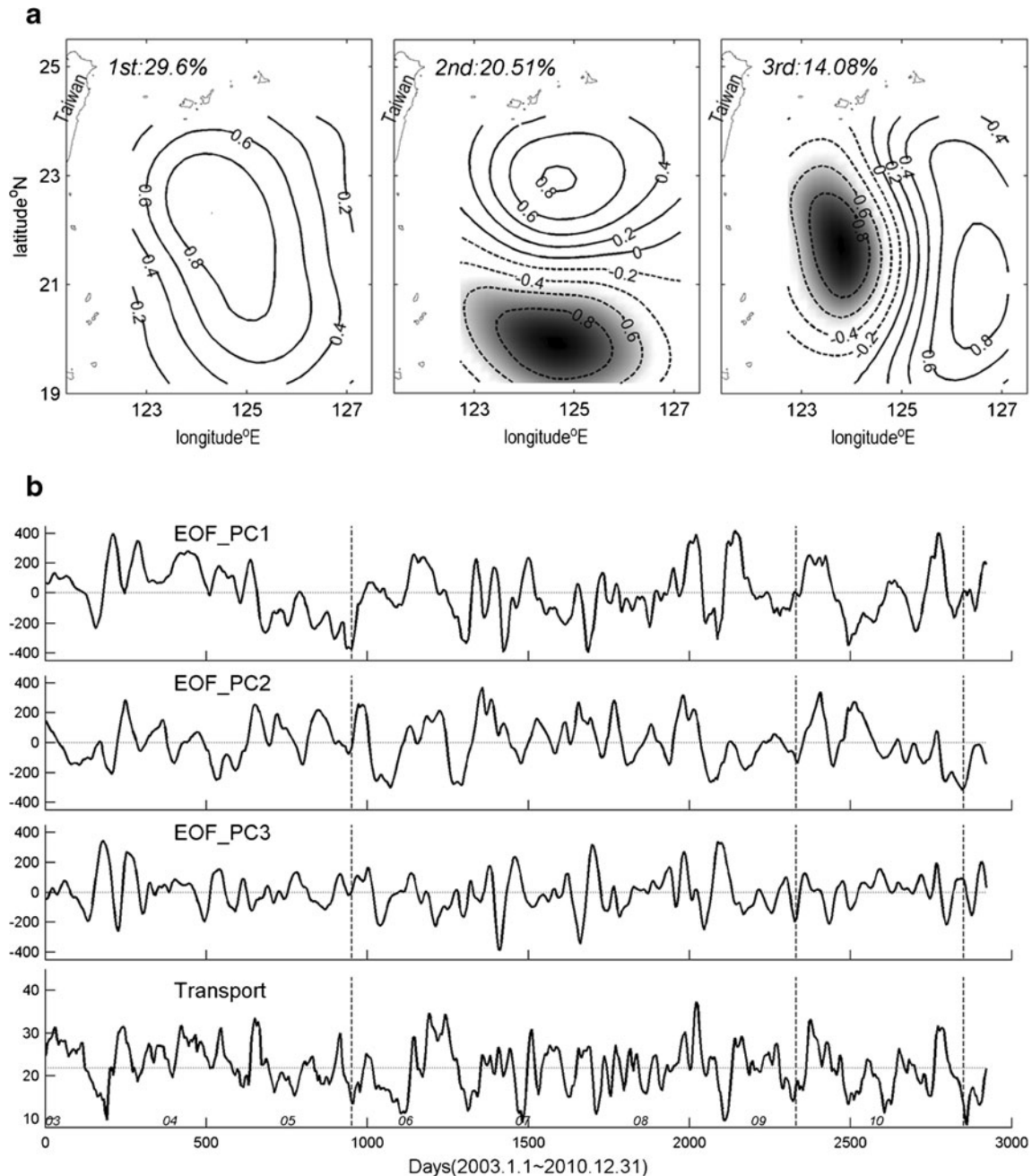


Fig. 5 **a** EOF amplitudes for dynamic heights: first mode (left), second mode (middle), and third mode (right). EOF amplitude is normalized and the negative region is shaded. Percentages of each mode are also shown. **b** EOF principal components (EOF_PC1–3) for dynamic heights

(top three plots) and Kuroshio transport (black, bottom plot; also shown in Fig. 4). Three vertical dashed lines marked at days 951, 2,331, and 2,851 correspond to modes 1, 3, and 2 in Fig. 10

standard deviation of T is large in the surface layer, increasing eastward. The model velocity and temperature structures agree well with the PCM-1 observations (Zhang et al. 2001).

The model's Kuroshio volume transport through the ETC is integrated along the red line marked in Fig. 1b. It ranges from 10 to 39 Sv, with dominant timescales of 70–150 days (Fig. 4). The 8-year mean volume transport is 24.4 Sv, with a standard deviation of 4.7 Sv. For the truncated PCM1 section (M1–M4), the model transport is 21.8 ± 5.3 Sv, which agrees well with 21.5 ± 4.1 Sv obtained from the 20-month PCM-1 observations (Johns et al. 2001). We noted that the PCM-1 period is relatively short and is not included in the reanalysis. The good agreement suggests that the Kuroshio transport is quite stationary in the interannual time scale. The total mean transport of 24.4 Sv also agrees with the Kuroshio transport in the East China Sea at 28° N, 24.0 ± 0.9 Sv, based on 13-month-long (November 2003 to November 2004) combined velocity and sea level observations (Andres et al. 2008b). Figure 4 also displays the latitude–time plot of the 8-year model dynamic heights. To include the shallower region, the reference level for dynamic heights is reduced to 500 m (DH_500). The boxes from the bottom to the top display the dynamic height contours in 17 – 25° N and 123 – 133° E. Westward-propagating eddies can be clearly identified from the time displacement in longitude. Zhang et al. (2001) suggested that the low Kuroshio volume transports are associated with the approaching anticyclonic eddies. In Fig. 4, several transport highs and lows are traced back to the approaching eddies. Our results indicate that the low (high) Kuroshio volume transports generally are associated with the westward-propagating cyclonic (anticyclonic) eddies. Only a few cases agree with Zhang et al. (2001), for example, the last case illustrated in Fig. 4 in which an approaching anticyclonic eddy caused a decreased Kuroshio transport.

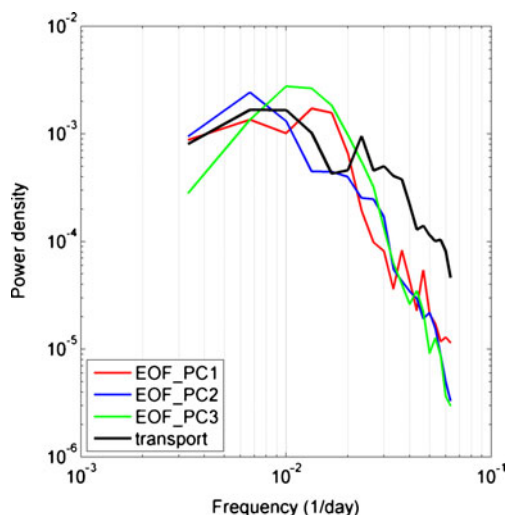


Fig. 6 Normalized energy spectra of EOF_PC1-3 and model Kuroshio transport

The dynamic height has a strong annual signal due to steric variations (Wang and Kobalinsky 1996; Stammer 1997). Since our study is primarily focused on mesoscale eddies, the annual harmonics which accounted for 40 % of the total variance are first removed. EOF analysis is then applied to the residual dynamic heights (rDH_500) in the model sub-domain bounded by 19 – 24° N and 122.7 – 127.2° E. Figure 5 shows spatial (amplitudes) and temporal (principal components, PCs) structures of the first three EOF modes which explain about 30, 20, and 14 % of the total variance, respectively. The first mode is a large single eddy of about 500 km in diameter, centered at 22° N. The second mode indicates two north–south counter-rotating eddies of about 400 km in diameter each, centered at 20° and 23° N, respectively. The third mode shows two east–west counter-rotating eddies of about 300 km in diameter each, centered at 123.5° and 126.5° E of 21° N, respectively. We noted that since the eddies are propagating from the open ocean, the EOF modal structures will be affected by the analysis domain. The box described earlier is chosen to focus on the region east of Taiwan and upstream of ETC, as only when eddies are close to ETC could high coherence with the Kuroshio transport be expected (Gawarkiewicz et al. 2011; Chang and Oey 2011). The large-scale eddy structures in STCC are examined later (Fig. 8).

Figure 6 shows the spectra of the first three principal components (PC1, PC2, and PC3; PC1–3) and the Kuroshio transport in the ETC. All four spectra show dominant energy peaks at around 70–150 days. Figure 7 displays the coherency and phase lags of the Kuroshio transport with PC1–3. For the

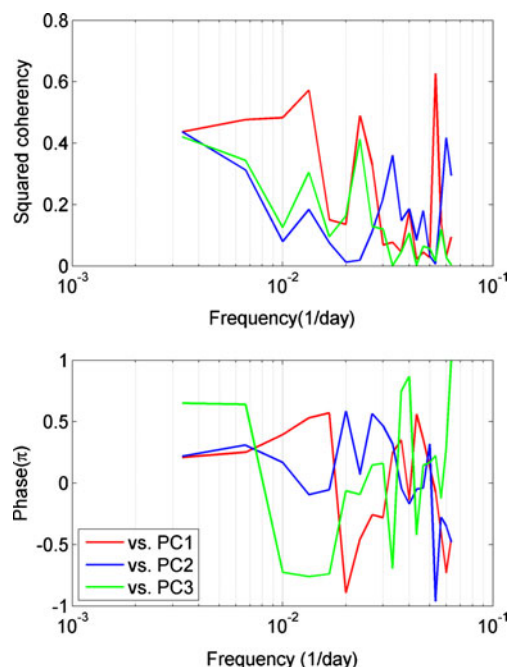


Fig. 7 Coherency and phase between EOF_PC1-3 and model Kuroshio transport

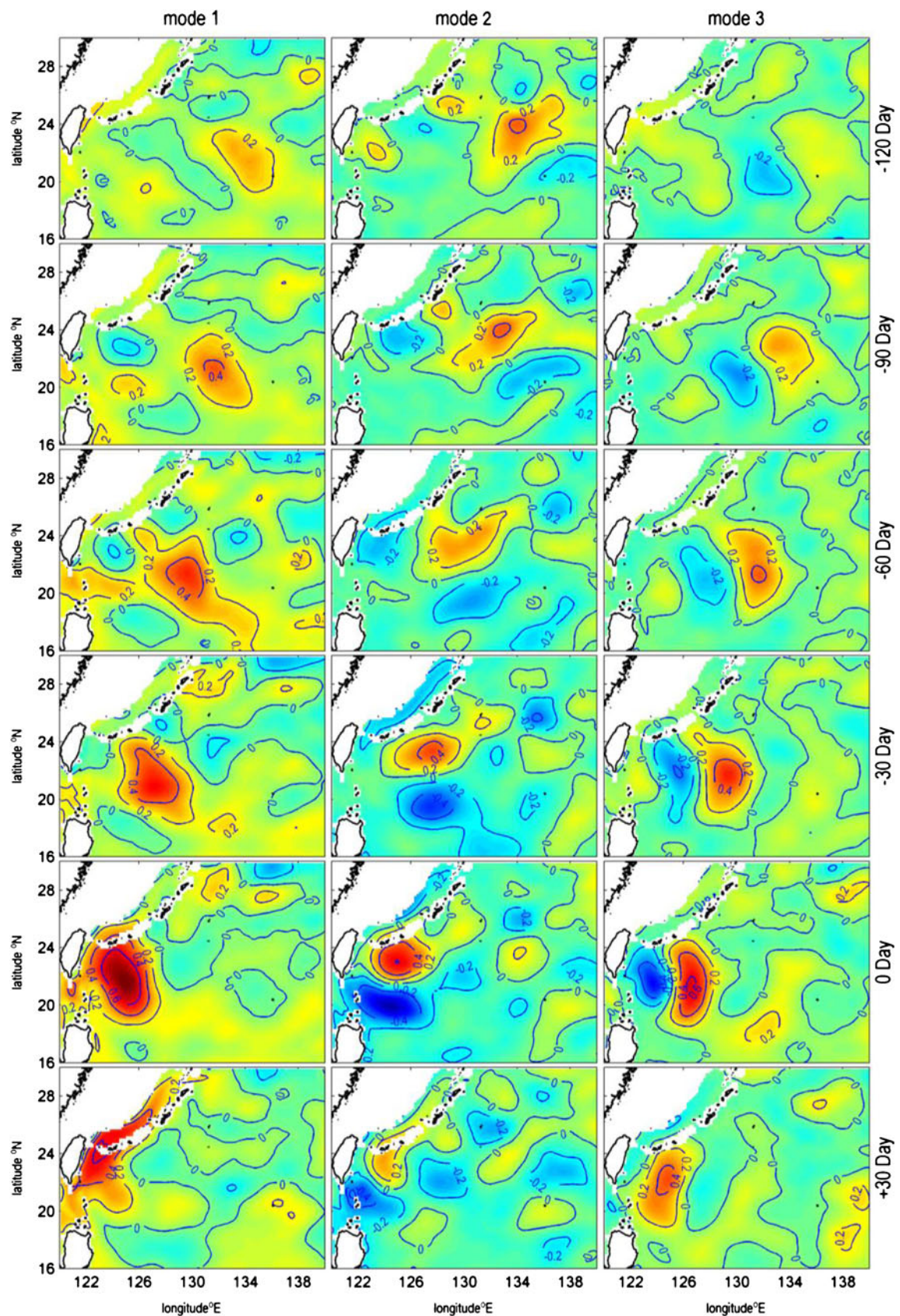
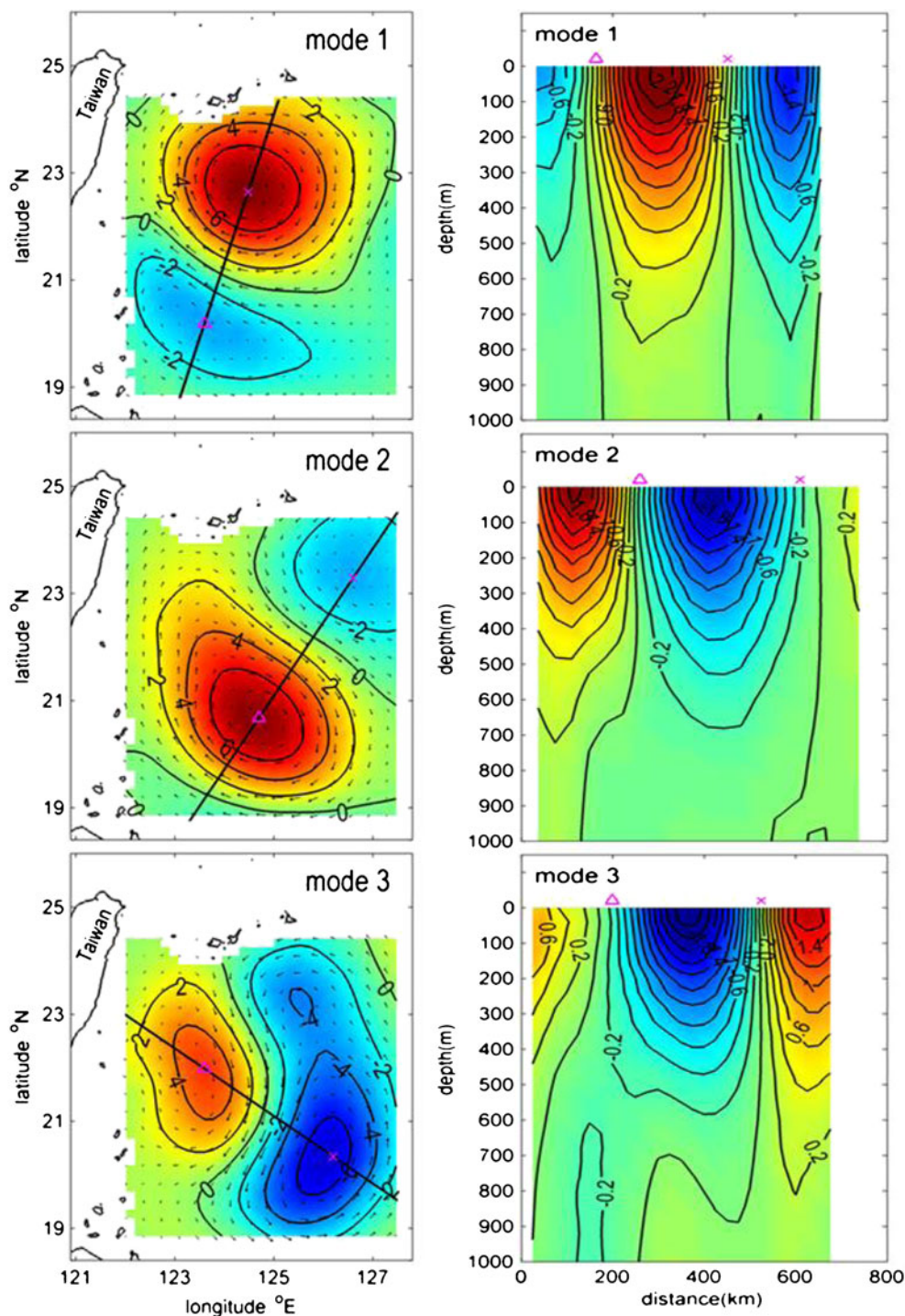


Fig. 8 Correlation coefficients between dynamic heights and EOF_PC1-3 from -120-day to +30-day lags with an interval of 30 days: first mode (left), second mode (middle), and third mode (right)

Fig. 9 Modal structures of dynamic height with three-dimensional velocity field from SVD analysis. *Left*, dynamic height (color shading with contour lines) and surface velocity (vectors) of the first three modes. *Right*, cross-section of normal velocity along the lines marked in the left panel. Triangle and multiplication symbol denote the eddy centers



first mode (Kuroshio transport vs. PC1), the coherency is high for periods >75 days, with the transport lagging PC1 by ~ 20 days. There is also a high coherency at 40 days with the transport leading PC1 by ~ 10 days. For the second mode, the coherency generally is low except at a very long period >150 days, with the transport lagging by 20–30 days. For the third mode, there is a high coherency at 75 days (transport leading by ~ 20 days) and 40 days (\sim zero lag),

respectively. The coherency is also high at a very long period >150 days. We noted that although the EOF modes are orthogonal in time domain, they could be coherent in certain frequency bands. For example, PC2 and PC3 are coherent at 70-day period (not shown). We choose the time domain EOF analysis in line with the previous studies. The time domain EOF analysis also allows for easy reconstruction of the ocean state (for example, Fig. 10).

In the EOF analysis, it is assumed that eddies are quasi-stationary within the analysis domain. To examine how the three EOF modes are related to dynamic heights in the open ocean, the principal components are lag-correlated, with residual dynamic heights (rDH_500) in the STCC. Figure 8 shows lag correlations every 30 days from -120 days to +30 days for the three EOF modes. With zero time lag, the correlation map shows spatial patterns that are basically the same as the EOF modal pattern. This indicates that the EOF analysis box indeed has captured the structures of the impinging eddies. Also, at zero time lag, PC1 and 2 are positively correlated with rDH_500 around southeast of ETC where Gawarkiewicz et al. (2011) found the maximum correlation between the Kuroshio transport and SSHA. With time lags, all three EOF modes can be tracked over a long distance/time in the STCC between 20 and 24° N. The phase speeds are ~8 km/day (8.16, 8.03 and 7.4 km/day, respectively, for PC1-3). Also, only the first mode seems to have significant impact further downstream in the East China Sea (at +30-day lag).

The model's three-dimensional velocity field is analyzed for the modal structure in the vertical. Instead of treating velocities as an independent field, SVD analysis is used to extract the flow patterns that are correlated with the dynamic height (Bretherton et al. 1992). For consistency, the annual cycle is also removed from the velocity field. The SVD is applied between the dynamic heights and horizontal velocities from the surface to 1,000 m in depth. Figure 9 shows the surface velocity and dynamic height patterns for the first three modes and the corresponding cross-sections of the normal velocity field. The time series of the first SVD mode is similar to EOF_PC2 (correlation coefficient, $\gamma=0.78$), the

second SVD mode to EOF_PC1 ($\gamma=0.77$), and the third SVD mode to EOF_PC3 ($\gamma=0.89$). The velocities are highly coherent in the vertical. The flow field extends to ~700 m in depth for modes 1 and 2 and to ~600 m for mode 3. Note that most of the vertical shears are confined to the upper 400 m. The deep penetration of the eddy motion is consistent with the findings of Roemmich and Gilson (2001) who found that the temperature anomalies associated with the “composite” warm/cold eddies extend to 600–800 m, with the largest temperature variations (and hence, the geostrophic velocity shears) in the upper 400 m.

A realization of the ocean state is generally a combination of the three leading EOF modes (64 % of total variance). There are instances though when a single mode dominates. Figure 9 illustrates examples when a single EOF mode is revealed from the concurrent Surface Velocity Program drifter trajectories; the latter were obtained from the enhanced GDP database maintained at the Scripps Institution of Oceanography (Niiler 2001). For each case, a snapshot of the model dynamic height (DH_500) is presented (with the area average removed for clarity), and all available drifter tracks within ± 30 days of the snapshot are superimposed. The time corresponding to each snapshot is marked in the EOF time series of Fig. 5b. The first case is at day 951 (2005/8/9) when the first EOF mode dominated. The situation is similar to SVD mode-2 (Fig. 9) in that a large cyclonic eddy (negative PC1) is present east of Taiwan. Two drifters (“red” and “blue”) closely traced the cyclonic eddy. The third drifter (“black”), however, was carried in a large anticyclonic circulation south of the cyclonic eddy. The second case is at day 2851 (2010/10/22) when the second EOF mode dominated (negative PC2). The drifters initially were all trapped

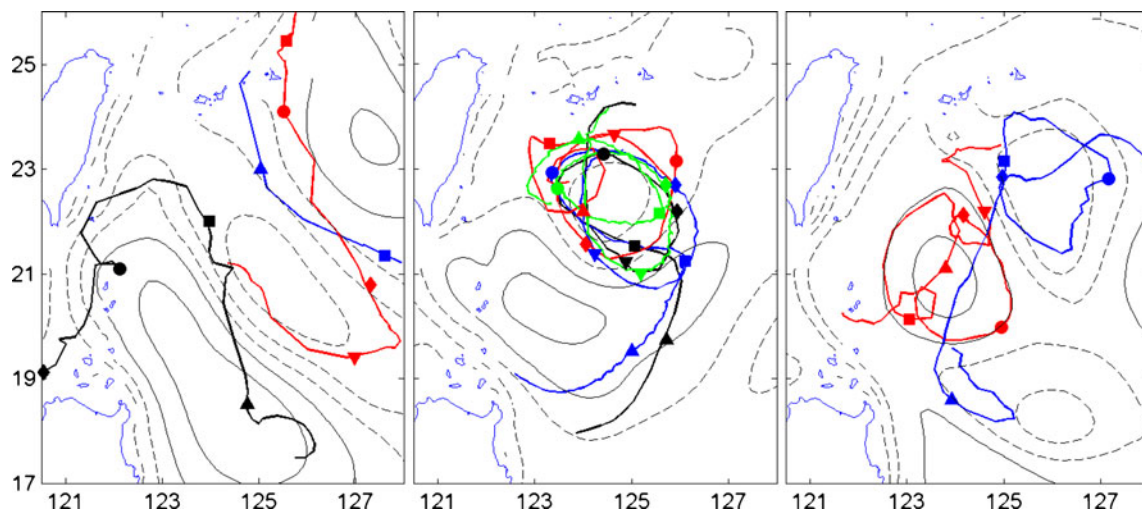


Fig. 10 Drifter trajectories from the GDP database and corresponding modeled dynamic height anomalies at days 951 (2005/8/9, *left*), 2,851 (2010/10/22, *middle*), and 2,331 (2009/5/20, *right*) for demonstrating EOF modes 1, 2, and 3, respectively. The domain-averaged dynamic height is subtracted of each plot. Solid (dashed) lines denote positive

(negative) values with a contour interval of 10 cm. Trajectories within ± 30 days are shown: -20 days (inverted filled triangle), -10 days (filled diamond), 0 day (filled circle), +10 days (filled square), and +20 days (filled triangle)

in a small cyclonic eddy, but two of them later escaped and followed a large anticyclonic eddy to the south. This period also corresponds to a (very) low Kuroshio transport (Fig. 5b) as a large portion of the Kuroshio flow is diverted eastward at the southern tip of Taiwan. The third case is at day 2,331 (2009/5/20) when the third EOF mode was relatively more important (negative PC3). At -10 day, the two drifters were closer by. The outer (“blue”) drifter made a loop around a cyclonic eddy but moved straight to the south between $+10$ and $+20$ days, indicating that the cyclonic eddy had evolved into a north–south elongated shape. Correspondingly, the inner (“red”) drifter made a spiral trajectory along an anticyclonic eddy. The north–south orientation of the eddy pair (east–west counter-rotating eddy pair) at $> +10$ days is consistent with the EOF mode 3.

4 Discussion

Using the 8-year (2003–2010) EASNFS analysis, the relationship between the Kuroshio volume transport and mesoscale eddies east of Taiwan is examined. The EOF analysis of model dynamic heights identifies three dominant modes, a single large eddy (PC1), a north–south-oriented eddy pair (PC2), and an east–west-oriented eddy pair (PC3). The corresponding velocity fields indicate that the eddies penetrate to a depth of 600–700 m, with strong velocity shears in the upper 400 m. The EOF modes and the Kuroshio volume transport have similar timescales of 70–150 days, and they generally are coherent with a lag of about 20 days.

Yang et al. (1999) suggested that the SSHA east of Taiwan were highly correlated with the Kuroshio transports estimated from sea level differences between Keelung and Ishigaki. Similarly, Gawarkiewicz et al. (2011) found maximum correlation between the Kuroshio transports and SSHA near Ishigaki. Yang et al. (1999) showed that an approaching anticyclonic/cyclonic eddy increased/decreased the Kuroshio transport. Their conclusion is supported by Andres et al. (2008a) who examined direct transport measurements during several eddy events. Zhang et al. (2001), on the other hand, suggested that the impinging anticyclonic eddies caused a decrease of the ETC transport. Ichikawa et al. (2008) obtained a similar result by correlating the surface Kuroshio velocity determined from the high-frequency radar measurements with the altimetry data. Our results reveal a more complicated situation of three different eddy modes affecting the Kuroshio transport. Yang et al. (1999) and Gawarkiewicz et al. (2011) can be related to PC1 and PC2, and Zhang et al. (2001) can be related to PC3. For PC1 and PC2, part of the Kuroshio transport is diverted by the cyclonic eddies to the east near the southern tip of Taiwan ($\sim 21^\circ$ N) (Fig. 10). For PC3, part of the Kuroshio transport is diverted by the anticyclonic eddies off the ETC along the east side of the Ryukyu Islands ($\sim 24^\circ$ N). As the first two modes are more

frequent, cyclonic eddies play the dominant role in decreasing the Kuroshio volume transport across the ETC (Fig. 3).

Ichikawa (2001) applied CEOF analysis to study the impact of eddies further north ($22\text{--}34^\circ$ N) using 15-month altimetry data. His first mode represents the annual signal ($\sim 40\%$ of variance), and the second mode which accounts for $\sim 24\%$ of variance has a timescale of ~ 6 months and plays the most important role in affecting the Kuroshio transport in the Tokara Strait. His second mode is related to the mesoscale eddies at 23° N, corresponding to our PC1 eddy. The lag correlation analysis indeed shows that only the PC1 eddy influences the Kuroshio transport in the East China Sea (Fig. 8).

The atmospheric reanalysis products such as the NCEP–NCAR Reanalysis (www.esrl.noaa.gov/psd/data/gridded/data.ncep.reanalysis.html) are routinely treated as the datasets. The reanalysis is advantageous as it employs a state-of-the-art analysis/forecast system to systematically assimilate the observations which are otherwise discrete in space and time. An oceanographic reanalysis product, on the other hand, is rarely available because global/regional ocean operational systems are still few. We demonstrate in this study the usefulness of EASNFS analysis in obtaining credible long-term Kuroshio volume transport estimates. Also, Qiu and Chen (2013) and Chang and Oey (2012) recently have emphasized the importance of large-scale wind stress curl in the STCC. Presumably, the impact of wind forcing on the Kuroshio volume transport could be also diagnosed from the EASNFS reanalysis which includes realistic atmospheric forcing.

Acknowledgments We appreciate comments from anonymous reviewers and Professor Tony Hirst that significantly improved the manuscript. This work originated from the Ph.D. research of IHL at National Taiwan University, Taipei. She wishes to thank her adviser, Professor Wen-Ssn Chuang, for his mentorship and guidance throughout this research. We gratefully acknowledge support by the National Science Council of Taiwan and the Aim for the Top University from the Ministry of Education. DSK was supported by ONR grant N00014-08WX-02-1170. LC was supported by ONR grant N00014-11-0347 and NOAA grant NA17RJ1231.

Open Access This article is distributed under the terms of the Creative Commons Attribution License which permits any use, distribution, and reproduction in any medium, provided the original author(s) and the source are credited.

References

- Andres M, Park JH, Wimbush M, Zhu XH, Chang KI, Ichikawa H (2008a) Study of the Kuroshio/Ryukyu current system based on satellite-altimeter and in situ measurements. *J Oceanogr* 64:937–950. doi:10.1007/s10872-008-0077-2
- Andres M, Wimbush M, Park JH, Chang KI, Lim BH, Watts DR, Ichikawa H, Teague WJ (2008b) Observation of Kuroshio flow variations in the East China Sea. *J Geophys Res* 113, C05013. doi:10.1029/2007JC004200

- Barron CN, Kara AB, Jacobs GA (2009) Objective estimates of westward Rossby wave and eddy propagation from sea surface height analyses. *J Geophys Res* 114, C03013. doi:10.1029/2008JC005004
- Bretherton CS, Smith C, Wallace JM (1992) An intercomparison of methods for finding coupled patterns in climate data. *J Climate* 5(6):541–560. doi:10.1175/1520-0442(1992)005<0541:AIOMFF>2.0.CO;2
- Carnes MR, Fox DN, Rhodes RC, Smedstad OM (1996) Data assimilation in a North Pacific Ocean monitoring and prediction system. In: Malanotte-Rizzoli P (ed) *Modern approaches to data assimilation in ocean modeling*. Elsevier Oceanography Ser 61:319–345. doi:10.1016/S0422-9894(96)80015-8
- Centurioni LR, Ohlmann JC, Niiler PP (2008) Permanent meanders in the California current system. *J Phys Oceanogr* 38(8):1690–1710. doi:10.1175/2008JPO3746.1
- Chang YL, Oey LY (2011) Interannual and seasonal variations of Kuroshio transport east of Taiwan inferred from 29 years of tide-gauge data. *Geophys Res Lett* 38, L08603. doi:10.1029/2011GL047062
- Chang YL, Oey LY (2012) The Philippines–Taiwan Oscillation: monsoonlike interannual oscillation of the subtropical–tropical western North Pacific wind system and its impact on the ocean. *J Climate* 25:1597–1618. doi:10.1175/JCLI-D-11-00158.1
- Chang YT, Tang TY, Chao S-Y, Chang M-H, Ko DS, Yang YJ, Liang W-D, McPhaden MJ (2010) Mooring observations and numerical modeling of thermal structures in the South China Sea. *J Geophys Res* 115, C10022. doi:10.1029/2010JC006293
- Chapman DC, Ko DS, Preller RH (2004) A high-resolution numerical modeling study of subtidal circulation in the northern South China Sea. *IEEE J Ocean Eng* 29:1087–1104. doi:10.1109/JOE.2004.838334
- Chelton DB, Schlax MG, Samelson RM, deSzoeke RA (2007) Global observations of large oceanic eddies. *Geophys Res Lett* 34, L15606. doi:10.1029/2007GL030812
- Ducet N, Le Traon PY, Reverdin G (2000) Global high-resolution mapping of ocean circulation from the TOPEX/Poseidon and ERS-1 and -2. *J Geophys Res* 105(C8):19477–19498
- Fox DN, Teague WJ, Barron CN, Carnes MR, Lee CM (2002) The Modular Ocean Data Assimilation System (MODAS). *J Atmos Oceanic Technol* 19:240–252. doi:10.1175/1520-0426(2002)019<0240:TMODAS>2.0.CO;2
- Gawarkiewicz G, Jan S, Lermusiaux P, McClean J, Centurioni L, Taylor K, Cornuelle B, Duda TF, Wang J, Yang YJ, Sanford T, Lien RC, Lee C, Lee MA, Leslie W, Haley Jr OJ, Niiler P, Gopalakrishnan G, Vélez-Belchi P, Lee DK, Kim YY (2011) Circulation and intrusions northeast of Taiwan: chasing and predicting uncertainty in the cold dome. *Oceanography* 24(4):110–121. doi:10.5670/oceanog.2011.99
- Hsin YC, Chiang TL, Wu CR (2011) Fluctuations of the thermal fronts off northeastern Taiwan. *J Geophys Res* 116, C10005. doi:10.1029/2011JC007066
- Hwang C, Wu CR, Kao R (2004) TOPEX/Poseidon observations of mesoscale eddies over the Subtropical Countercurrent: kinematic characteristics of an anticyclonic and a cyclonic eddy. *J Geophys Res* 109, C08013. doi:10.1029/2003JC002026
- Ichikawa K (2001) Variation of the Kuroshio in the Tokara Strait induced by meso-scale eddies. *J Oceanogr* 57:55–68. doi:10.1023/A:1011174720390
- Ichikawa K, Tokeshi R, Kashima M, Sato K, Matsuoka T, Kojima S, Fujii S (2008) Kuroshio variations in the upstream region as seen by HF radar and satellite altimetry data. *Int J Remote Sens* 29(21):6417–6426. doi:10.1080/01431160802175454
- Jacobs GA, Ko DS, Ngodock H, Preller RH, Riedlinger SK (2005) Synoptic forcing of the Korea Strait transport. *Deep-Sea Res II* 52:1490–1504. doi:10.1016/j.bbr.2011.03.031
- Johns WE, Lee TN, Zhang D, Zantopp R, Liu CT, Yang Y (2001) The Kuroshio east of Taiwan: moored transport observations from the WOCE PCM-1 array. *J Phys Oceanogr* 31:1031–1053. doi:10.1175/1520-0485(2001)031<1031:TKEOTM>2.0.CO;2
- Jerlov NG (1964) Optical classification of ocean water. In: Tyler JE (ed) *Physical aspects of light in the sea*. U Hawaii Press, Honolulu, pp 45–49
- Keen TR, Ko DS, Slingerland RL, Riedlinger S (2006) Potential transport pathways of terrigenous material in the Gulf of Papua. *Geophys Res Lett* 33, L04608. doi:10.1029/2005GL025416
- Ko DS, Chao SY, Huang P, Lin SF (2009) Anomalous upwelling in Nan Wan: July 2008. *Terr Atmos Ocean Sci* 20(6):839–852. doi:10.3319/TAO.2008.11.25.01(Oc)
- Ko DS, Martin PJ, Rowley CD, Preller RH (2008) A real-time coastal ocean prediction experiment for MREA04. *J Mar Syst* 69:17–28. doi:10.1016/j.jmarsys.2007.02.022
- Kobashi F, Kawamura H (2002) Seasonal variation and instability nature of the North Pacific Subtropical Countercurrent and the Hawaiian Lee Countercurrent. *J Geophys Res* 107(C11):3185. doi:10.1029/2001JC001225
- Leaman KD, Vertes PS, Atkinson LP, Lee TN, Hamilton P, Waddell E (1995) Transport, potential vorticity and current/temperature structure across Northwest Providence and Santaren Channels and the Florida Current off Cay Sal Bank. *J Geophys Res* 100(C5):8561–8569. doi:10.1029/94JC01436
- Lee IH, Wang DP, Chung WS (2003) Structure and propagation of a large cyclonic eddy in the western North Pacific from analysis of XBT and altimetry data and numerical simulation. *Terrestrial, Atmospheric and Oceanic Sci* 14(2):183–200
- Lee TN, Johns WE, Liu CT, Zhang D, Zantopp R, Yang Y (2001) Mean transport and seasonal cycle of the Kuroshio east of Taiwan with comparison to the Florida Current. *J Geophys Res* 106(C10):22143–22158. doi:10.1029/2000JC000535
- Lin II, Wu CC, Pun IF, Ko DS (2008) Upper ocean thermal structure and the western North Pacific category-5 typhoons, part I: ocean features and category-5 typhoon's intensification. *Mon Wea Rev* 136:3288–3306. doi:10.1175/2008MWR2277.1
- Liu Z, Gan J (2012) Variability of the Kuroshio in the East China Sea derived from satellite altimetry data. *Deep-Sea Res I* 59:25–36. doi:10.1046/j.dsr.2011.10.008
- Martin PJ (2000) Description of the Navy Coastal Ocean Model Version 1.0. Tech Rep NRL/FR/7322-00-9962: 42 pp
- Maximenko N, Niiler PP, Rio MH, Melnichenko O, Centurioni L, Chambers D, Zlotnicki V, Galperin B (2009) Mean dynamic topography of the ocean derived from satellite and drifting buoy data using three different techniques. *J Atmos Oceanic Technol* 26:1910–1919. doi:10.1175/2009JTECHO672.1
- Niiler PP (2001) The world ocean surface circulation. In: Church J, Siedler G, Gould J (eds) *Ocean circulation and climate: observing and modeling the global ocean*. Academic, San Diego, pp 193–204
- Qiu B (1999) Seasonal eddy field modulation of the North Pacific Subtropical Countercurrent: TOPEX/Poseidon observations and theory. *J Phys Oceanogr* 29:1670–1685. doi:10.1175/1520-0485(2001)031<0675:ETOHAT>2.0.CO;2
- Qiu B, Chen S (2010) Interannual variability of the North Pacific Subtropical Countercurrent and its associated mesoscale eddy field. *J Phys Oceanogr* 40:213–225. doi:10.1175/2009JPO4285.1
- Qiu B, Chen S (2013) Concurrent decadal mesoscale eddy modulations in the Western North Pacific Subtropical Gyre. *J Phys Oceanogr* 43:344–358. doi:10.1175/JPO-D-12-0133.1
- Rhodes RC, Hurlburt HE, Wallcraft AJ, Barron CN, Martin PJ, Smedstad OM, Cross S, Metzger EJ, Shriver J, Kara A, Ko DS (2002) Navy real-time global modeling system. *Oceanography* 15(1):29–43. doi:10.5670/oceanog.2002.34
- Rio MH, Guinehut S, Larnicol G (2011) New CNES-CLS09 global mean dynamic topography computed from the combination of GRACE data, altimetry, and in situ measurements. *J Geophys Res* 116, C07018. doi:10.1029/2010JC006505

- Roemmich D, Gilson J (2001) Eddy transport of heat and thermocline waters in the North Pacific: a key to interannual/decadal climate variability. *J Phys Oceanogr* 31:675–687. doi:[10.1175/1520-0485\(2001\)031<0675:ETOHAT>2.0.CO;2](https://doi.org/10.1175/1520-0485(2001)031<0675:ETOHAT>2.0.CO;2)
- Rosmond TE (1992) The design and testing of the Navy Operational Global Atmospheric Prediction System. *Weather Forecast* 7:262–272. doi:[10.1175/1520-0434\(1992\)](https://doi.org/10.1175/1520-0434(1992)7<262:DOGAPS>2.0.CO;2)
- Rudnick DL, Jan S, Centurioni L, Lee CM, Lien RC, Wang J, Lee DK, Tseng RS, Kim YY, Chern CS (2011) Seasonal and mesoscale variability of the Kuroshio near its origin. *Oceanography* 24(4):52–63
- Scharffenberg MG, Stammer D (2010) Seasonal variations of the large-scale geostrophic flow field and eddy kinetic energy inferred from the TOPEX/Poseidon and Jason-1 tandem mission data. *J Geophys Res* 115, C02008. doi:[10.1029/2008JC005242](https://doi.org/10.1029/2008JC005242)
- Stammer D (1997) Steric and wind-induced changes in TOPEX/POSEIDON large-scale sea surface topography observations. *J Geophys Res* 102(C9):20987–21009. doi:[10.1029/97JC01475](https://doi.org/10.1029/97JC01475)
- Teague WJ, Ko DS, Jacobs GA, Perkins HT, Book JW, Smith SR, Chang KL, Suk MS, Kim K, Lyu SJ, Tang TY (2006) Currents through the Korea/Tsushima Strait: a review of LINKS observations. *Oceanography* 19(3):50–63. doi:[10.5670/oceanog.2006.43](https://doi.org/10.5670/oceanog.2006.43)
- Wang DP, Oey LY, Ezer T, Hamilton P (2003) Near-surface currents in DeSoto Canyon (1997–99): comparison of current meters, satellite observation, and model simulation. *J Phys Oceanogr* 33(1):313–326. doi:[10.1175/1520-0485\(2003\)033<0313:NSCIDC>2.0.CO;2](https://doi.org/10.1175/1520-0485(2003)033<0313:NSCIDC>2.0.CO;2)
- Wang L, Kobalinsky CJ (1996) Annual variability of the subtropical recirculation in the North Atlantic and North Pacific: a TOPEX/Poseidon study. *J Phys Oceanogr* 26(11):2462–2479. doi:[10.1175/1520-0485\(1996\)026<2462:AVOTSR>2.0.CO;2](https://doi.org/10.1175/1520-0485(1996)026<2462:AVOTSR>2.0.CO;2)
- Yang Y, Liu CT, Hu JH, Koga M (1999) Taiwan Current (Kuroshio) and impinging eddies. *J Oceanogr* 55:609–617. doi:[10.1023/A:1007892819134](https://doi.org/10.1023/A:1007892819134)
- Zhang D, Lee TN, Johns WE, Liu CT, Zantopp R (2001) The Kuroshio East of Taiwan: modes of variability and relationship to interior ocean mesoscale eddies. *J Phys Oceanogr* 31:1054–1074. doi:[10.1175/1520-0485\(2001\)031<1054:TKEOTM>2.0.CO;2](https://doi.org/10.1175/1520-0485(2001)031<1054:TKEOTM>2.0.CO;2)
- Zhu XH, Ichikawa H, Ichikawa K, Takeuchi K (2004) Volume transport variability southeast of Okinawa Island estimated from satellite altimeter data. *J Oceanogr* 60:953–962. doi:[10.1007/s10872-005-0004-8](https://doi.org/10.1007/s10872-005-0004-8)